

Interpretation of the coronal magnetic field configuration of the Sun *

Bo Li^{1,2}, Xing Li³ and Hui Yu¹

¹ Shandong Provincial Key Laboratory of Optical Astronomy & Solar-Terrestrial Environment, School of Space Science and Physics, Shandong University at Weihai, Weihai 264209, China; bbl@sdu.edu.cn

² State Key Laboratory of Space Weather, Chinese Academy of Sciences, Beijing 100190, China

³ Institute of Mathematics & Physics, Aberystwyth University, Aberystwyth SY23 3BZ, UK

Received 2012 April 23; accepted 2012 June 4

Abstract The origin of the heliospheric magnetic flux on the Sun, and hence the origin of the solar wind, is a topic of hot debate. While the prevailing view is that the solar wind originates from outside the coronal streamer helmets, there also exists the suggestion that the open magnetic field spans a far wider region. Without the definitive measurement of the coronal magnetic field, it is difficult to unambiguously resolve the conflict between the two scenarios. We present two 2-dimensional, Alfvénic-turbulence-based models of the solar corona and solar wind, one with and the other without a closed magnetic field region in the inner corona. The purpose of the latter model is to test whether it is possible to realize a picture suggested by polarimetric measurements of the corona using the Fe XIII 10747 Å line, where open magnetic field lines seem to penetrate the streamer base. The boundary conditions at the coronal base are able to account for important observational constraints, especially those on the magnetic flux distribution. Interestingly, the two models provide similar polarized brightness (pB) distributions in the field of view (FOV) of SOHO/LASCO C2 and C3 coronagraphs. In particular, a dome-shaped feature is present in the C2 FOV even for the model without a closed magnetic field. Moreover, both models fit the Ulysses data scaled to 1 AU equally well. We suggest that: 1) The pB observations cannot be safely taken as a proxy for the magnetic field topology, as is often implicitly assumed. 2) The Ulysses measurements, especially the one showing a nearly uniform distribution with heliocentric latitude of the radial magnetic field, do not rule out the ubiquity of open magnetic fields on the Sun.

Key words: Sun: corona — Sun: magnetic fields — solar wind

1 INTRODUCTION

Identifying the source regions of the heliospheric magnetic flux, and hence those of the solar wind, is a long standing issue in solar physics (see e.g., Schwenn 2006; Wang 2009). The difficulties

* Supported by the National Natural Science Foundation of China.

associated with this identification are mainly due to the difficulty in directly measuring the solar coronal magnetic field, which is essential in most of the schemes mapping the in situ solar winds to their coronal sources (Levine et al. 1977; Wang & Sheeley 1990; Neugebauer et al. 1998, 2002; Wang & Sheeley 2006; Abbo et al. 2010, to name but a few). Although advances on polarimetric measurements with coronal emission lines have been recently made (Habbal et al. 2001, 2003; Lin et al. 2004; Liu 2009), the coronal magnetic field remains largely unknown (e.g., Cargill 2009).

Without detailed, quantitative measurements, the coronal magnetic field has been commonly constructed via numerical extrapolation. While all available schemes use the photospheric magnetic field as a boundary input, they differ substantially in how to treat the effects of electric currents on the global coronal magnetic field in a volume bounded by the photosphere and some outer boundary. The electric currents may be neglected altogether (e.g., the potential field source surface (PFSS) model by Schatten et al. 1969; Altschuler & Newkirk 1969), they may be assumed to be purely horizontal (e.g., the current sheet source surface model by Zhao & Hoeksema 1995), or flow exclusively along magnetic field lines (e.g., the force-free model by Tadesse et al. 2009), or both the volumetric and sheet currents are self-consistently computed as a product of the plasma properties (the magnetohydrodynamic (MHD) models by e.g., Lionello et al. 2009). Polarized brightness (pB) images of the solar corona, routinely obtained with space-borne and ground-based coronagraphs, often guide the extrapolation schemes such that the resultant magnetic field configuration matches the available pB images. This implies that the density structures, as manifested in the pB images, reflect the magnetic topology in the inner corona. In addition, the usually dome-shaped streamer helmets, the most prominent feature in pB images, are seen as being comprised of closed magnetic fields. It follows that the bulk of the solar wind originates from the open field regions outside streamer helmets, even though the precise fraction by which coronal holes and the quiet Sun contribute to the solar wind is debatable (Kopp 1994; Hu et al. 2003, and references therein).

However, this scenario is not universally accepted. A distinct picture has been advocated in which the solar wind flows along the ubiquitous open magnetic field lines that are not limited to coronal holes or the quiet Sun, but come from throughout the Sun (Woo & Habbal 1999, 2003; Woo et al. 2004) (see also Woo & Druckmüllerová 2008). Interestingly, the arguments initially raised to support this picture also came from density measurements. By combining the near-Sun pB values with radio occultation measurements as well as in situ solar wind data, Woo & Habbal (1999) showed that the signatures of coronal sources are preserved in the measured solar wind away from the Sun, contending that these density imprints are propagating almost radially. Further support for this scenario comes from the fact that the white light images of the Sun at total eclipses, when properly processed, exhibit a rich set of filamentary structures that extend almost radially from the solar surface (see fig. 1 in Woo & Habbal 2003). Supposing these fine structures trace the magnetic field lines, this would suggest that some coronal magnetic field lines penetrate the dome-shaped streamer base. More importantly, these apparently open magnetic fields were also seen in the polarimetric measurements of the inner corona using the Fe XIII 10747 Å line (see figures in Habbal et al. 2001, 2003). Carefully addressing observational complications such as collisional depolarization and the Van Fleck effect, Habbal et al. (2001) argued that the largely radially aligned polarization vectors may indeed reflect a coronal magnetic field that is predominantly radial.

Given the importance of addressing the origin of the open magnetic flux of the heliosphere, it is surprising to see that while the traditional scenario has been extensively incorporated into numerical studies originated by Pneuman & Kopp (1971) (also see Lionello et al. 2009, and references therein), the scenario proposed by Woo & Habbal (2003) has not been modeled quantitatively. Here we wish to implement this scenario in a numerical model, thereby testing it against two fundamental constraints that the traditional scenario can readily satisfy: one is the appearance of a dome-shaped bright feature in the pB images, and the other is the fact established by Ulysses measurements that the radial magnetic field strength B_r is nearly uniform with latitude beyond 1 AU (Smith & Balogh 1995; Smith et al. 2001). Note that the latter fact was used to refute the suggestion of a largely

radially expanding solar wind (Smith et al. 2001), as the magnetic flux near the Sun is obviously nonuniform (e.g., Svalgaard et al. 1978; Vázquez et al. 2003). Before proceeding, we note that from the SOHO/EIT images, it is obvious that there are a myriad of low-lying loop-like structures in the corona. As suggested by Habbal et al. (2001), a large-scale closed magnetic field (the “nonradial” component in their paper) may also help shape the large-scale corona. To simplify our treatment, we will simply try to answer one question: can a dome-shaped bright feature show up in a magnetic configuration where there is no closed field at all? In essence, this is equivalent to saying that we are interested in the region somewhere above the layer below which loops abound in the SOHO/EIT images, and beyond which the contribution from closed magnetic fields is assumed to be negligible.

In what follows, we will present two numerical models that differ in terms of their magnetic field configuration in the inner corona, one with and the other without a closed field region. Both models are able to incorporate the essential observational constraints near the coronal base, especially the latitudinal dependence of the radial magnetic field. We then construct pB maps to see whether they display features similar to what is seen in white light observations. Moreover, model results are also compared with several crucial parameters observed in situ. The models are described in Section 2, results from the numerical computations are given in Section 3, and Section 4 concludes this paper.

2 DESCRIPTION OF THE NUMERICAL MODEL

Assuming azimuthal symmetry, our models solve, in the meridional plane (r, θ) , the standard two-fluid MHD equations identical to those in Hu et al. (2003). Here r is the heliocentric distance, and θ is the colatitude. The protons are heated by a flux of Alfvén waves dissipated at the Kolmogorov rate $Q_{\text{kol}} = \rho \langle \delta v^2 \rangle^{3/2} / L_c$, where $\langle \delta v^2 \rangle^{1/2}$ is the rms amplitude of velocity fluctuations of the wave field, and $\rho = nm_p$ is the mass density in which n is the number density and m_p the proton mass. The dissipation length L_c is given by $L_c = g(\psi) L_0 (B_{b,p}/B)^{1/2}$ where B denotes the magnetic field strength, the subscript b represents the value at the coronal base, and $B_{b,p}$ and L_0 are respectively B and L_c evaluated at the pole ($r = 1 R_\odot$ and $\theta = 0^\circ$). In addition, $g(\psi)$ describes the dependence of L_c on ψ , the magnetic flux function which labels flow tubes. For the electrons, classical field-aligned heat conduction is considered. While not directly heated, electrons receive part of the dissipated wave energy via Coulomb collisions with protons, whose heat conduction is neglected. With properly specified boundary conditions and given $g(\psi)$ as well as L_0 , our numerical computation starts with an arbitrary initial state and runs until a steady state is found. This steady state does not rely on the initial state but is solely determined by $g(\psi)$, L_0 and the boundary conditions at the coronal base. As a product, the computation yields a global distribution in the $r-\theta$ plane of the proton number density n , the radial and latitudinal components of the proton velocity v_r and v_θ respectively, the magnetic flux function ψ , the electron and proton temperatures T_e and T_p respectively, as well as the wave pressure $p_w = \rho \langle \delta v^2 \rangle / 2$. The magnetic field \mathbf{B} is then obtained via $\mathbf{B} = \nabla\psi \times \mathbf{e}_\phi / r \sin\theta$, where \mathbf{e}_ϕ represents the unit vector along the azimuthal direction.

The numerical scheme has been described in detail by Hu et al. (2003). The computational domain extends from the coronal base ($1 R_\odot$) to 1 AU, and from the pole (colatitude $\theta = 0^\circ$) to equator ($\theta = 90^\circ$). Both the pole and equator are taken as symmetrical boundaries. At the top boundary (1 AU), all dependent variables are linearly extrapolated for simplicity. On the other hand, at the coronal base, the proton density n , magnetic flux ψ , temperatures (T_e and T_p) and wave pressure p_w are all fixed. The velocity components v_r and v_θ are derived from the requirements that \mathbf{v} is aligned with \mathbf{B} , and mass flux is conserved along magnetic field lines. What distinguishes the two models lies in how the values for n , T_e , T_p , ψ , and p_w are imposed at the coronal base, and also in how $g(\psi)$ is prescribed. In what follows let the two models be labeled FO (fully open) and PO (partially open), respectively.

Figure 1 shows the distribution at the coronal base with colatitude θ of (a) the density n and temperature T (the temperatures of the protons and electrons are assumed to be equal at the base),

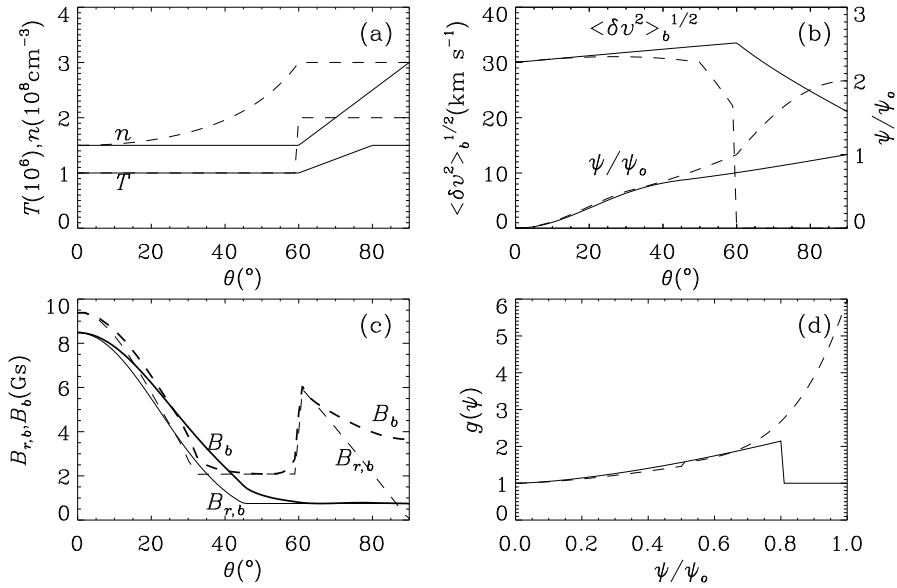


Fig. 1 Boundary conditions imposed at the coronal base. (a) Electron density n and temperature T . Electrons and protons are assumed to have identical temperatures at the base. (b) Wave amplitude $\langle \delta v^2 \rangle^{1/2}$ and magnetic flux ψ in units of the open flux ψ_0 . (c) Radial magnetic field B_r and the total field strength B . (d) Behavior of the function $g(\psi)$ that dictates the wave dissipation length (please see text). Model FO is given by the continuous curves while model PO by the dashed ones.

(b) the wave amplitude $\langle \delta v^2 \rangle^{1/2}$ and magnetic flux given by ψ/ψ_0 , with ψ_0 being the total open flux, (c) the radial magnetic field B_r (thin curves) and magnetic field strength B (thick curves).

Figure 1(d) describes the behavior of $g(\psi)$. The solid lines are for model FO whereas the dashed lines describe model PO. For model PO, the choice of the latitudinal profile for (n, T_e, T_p, ψ, p_w) and that of $g(\psi)$ have been described in considerable detail in Hu et al. (2003), and therefore we put more emphasis on the justification of model FO. Let us start with the distribution of the magnetic flux function ψ . Both computations adopt the same value for the open flux $\psi_0 = 7.37 \times 10^{21}$ Mx, which corresponds to an average radial magnetic field of 3.3γ at 1 AU, compatible with the Ulysses measurements (Smith & Balogh 1995; Smith et al. 2001).

Figure 1(b) indicates that in model PO the total flux (ψ at equator) is assumed to be twice the open flux, and only the portion $\theta \leq 60^\circ$ of the solar surface contributes to the open flux. However, in model FO the interplanetary magnetic flux ψ_0 is assumed to emerge from all over the Sun, evidenced by the fact that the magnetic flux ψ at the equator equals the total open flux ψ_0 . Actually, the distribution of ψ with θ derives from the θ -profile of B_r at the coronal base, presented by the thin curves in Figure 1(c). The specific form of ψ adopted in FO reflects the observed fact that $B_{r,b} \propto \cos^7 \theta$ for $\theta \lesssim 45^\circ$ and is roughly constant elsewhere, established by the measurements from Kitt Peak synoptic magnetograms at solar minima (see Vázquez et al. 2003, fig. 3).

Figure 1(a) indicates that the two models do not differ substantially in the profiles of n and T . While model PO uses a step function in T with T jumping from 1 MK to 2 MK at $\theta = 60^\circ$, model FO adopts a somewhat smoother distribution of T with a ramp connecting two values of 1 and 1.5 MK, with the ramp spanning the range $60^\circ \leq \theta \leq 80^\circ$. It suffices to note that the quoted value of 1 MK is compatible with electron temperatures in coronal holes, and values of 1.5 and 2 MK

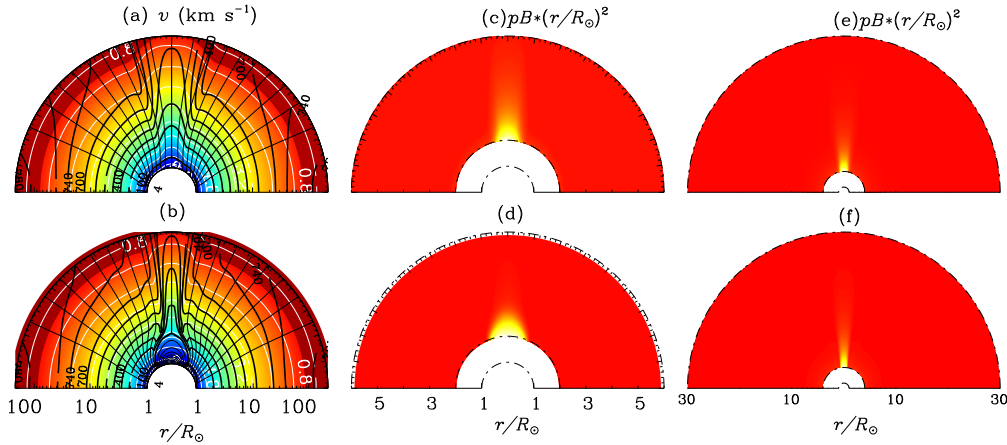


Fig. 2 Global solar wind models where the magnetic field is fully open (top panels, model FO) and partially open (bottom panels, model PO). (a) and (b) Outflow speed v (thick black contours) superimposed on the density map (logarithm of density $\log n$). The white curves represent the $\log n$ contours. The thin black curves in the background are magnetic field lines equally spaced by $0.1\psi_o$, with ψ_o being the open flux. The remaining panels give the pB maps computed from the modeled densities n . pB is measured in units of B_\odot , the solar mean disk brightness. Note that $\text{pB}(r/R_\odot)^2$ is plotted instead of pB. Panels (c) and (d) are for the heliocentric range of $1 - 6R_\odot$, while (e) and (f) are for $4 - 30 R_\odot$. Note that the two regions correspond to the FOV for LASCO C2 and C3, respectively.

are in line with electron temperatures in the quiet Sun and inside the streamer base (Habbal et al. 1993; Li et al. 1998). For the profile of n , model PO uses a distribution which is uniform in the range $60^\circ \leq \theta \leq 90^\circ$, but decreases with decreasing θ for the rest of the solar surface. The quoted values of $1.5 \times 10^8 \text{ cm}^{-3}$ at the pole and $3 \times 10^8 \text{ cm}^{-3}$ at the equator both agree with the spectroscopic measurements (Habbal et al. 1993; Li et al. 1998). On the other hand, the wave amplitudes given in Figure 1(b) for both models are below the upper limit derived spectroscopically (Esser et al. 1999). We note that in model PO, the waves are assumed to be absent in the closed field regions. Finally, as there is no direct constraint on the correlation length of the turbulent Alfvén waves, the $g(\psi)$ curves given in Figure 1(d) are found by a trial-and-error procedure such that the model results are presented that best match observations.

3 NUMERICAL RESULTS

The numerical results for models FO and PO are presented in the top and bottom panels of Figure 2, respectively. Figure 2(a) and (b) gives the contours of the outflow speed v (thick black curves) superimposed on the distribution of the density n . Moreover, the white contours are for $\log n$, and the background thin curves represent the magnetic field lines equally spaced by $0.1\psi_o$. The polarized brightness maps (in units of the mean disk brightness B_\odot of the Sun) are displayed for the heliocentric range of $2 - 6 R_\odot$ (Fig. 2(c) and (d)) and $4 - 30 R_\odot$ (Fig. 2(e) and (f)), corresponding to the FOV of the LASCO C2 and C3 coronagraphs onboard SOHO. These pB data are computed from the modeled densities using the standard formulae given in e.g., van de Hulst (1950); Vázquez et al. (2003). It is obvious from Figure 2(a) and (b) that both models produce an outflow field characterized by a narrow wedge of slow and dense wind ($v \leq 400 \text{ km s}^{-1}$) embedded in the fast wind. In model PO, a region associated with a closed magnetic field can be seen whose tip is located at around $3.5 R_\odot$.

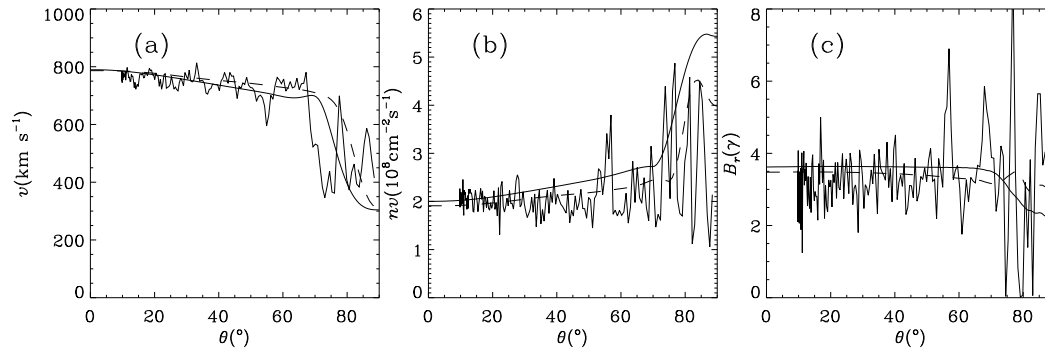


Fig. 3 Comparison with Ulysses data of derived latitudinal distributions of various parameters. (a) Outflow speed v . (b) Flux density nv . (c) Radial component of the magnetic field B_r . Model FO is given by the continuous lines, whereas model PO is given by the dashed lines. Moreover, in situ measurements by Ulysses are given by the light continuous lines.

However, model FO does not possess such a region, and the solar wind flows from throughout the Sun. Despite this, both models produce similar pB maps in the two different heliocentric ranges. In particular, Figure 2(c) and (d) both display a dome-like bright feature. Although in model PO this feature is associated with the trapping of plasmas in closed field regions, in model FO it is due to the fact that the density in the region near the equator decreases more slowly with radial distance than n does in the polar region. Moreover, the high-latitude magnetic field lines can be seen to bend towards the equator to relax the latitudinal gradient in the magnetic pressure. From this we conclude that, even though the magnetic field lines in model FO are not purely radial, the surprising linear polarization measurements with the Fe XIII 10747 Å line placed in the context of the pB measurements (e.g., the west limb in fig. 1 of Habbal et al. 2001) can be understood: the large-scale bright features may not reflect properties of the closed field regions, but rather are associated with the open field lines that penetrate them.

Figure 3 compares the latitudinal distribution at 1 AU of (a) the outflow speed v , (b) the flux density nv and (c) the radial magnetic field B_r , derived from the two models. Model PO (FO) is described by the dashed (solid) curves. Also plotted are the daily averages of Ulysses data during the first half of the fast latitudinal scan from 1994 September 12 to 1995 March 4. The two models, although having distinct magnetic configurations in the inner corona, provide equally good fits to the Ulysses data. One may say that while the proton flux density nv in model FO seems to be slightly larger than the measured values near the equator, it is nonetheless within the ranges typically measured in situ (fig. 4 in McComas et al. 2000). Concerning the distribution of B_r , model FO actually agrees with the Ulysses measurements better than model PO does. Furthermore, it is interesting to see that B_r hardly displays any latitudinal dependence in the fast wind region. But this is certainly not the case at the coronal base, shown in Figure 1(c). The relaxation of the latitudinal gradient in B_r can be understood from the force balance condition in the direction perpendicular to the ambient magnetic field. When the magnetic field becomes largely radial, this condition reduces to the case that $(\beta + 1) B^2 / 8\pi$ is latitude independent, where $\beta = 8\pi(p_e + p_p + p_w) / B^2$, p_e and p_p are respectively the electron and proton pressures, and p_w is the wave pressure. It turns out that this happens at some distance where $\beta \ll 1$ holds in both models. Consequently, the magnetic field should exhibit little latitudinal variation from there on. This relaxation process necessarily leads to a significant non-radial component of the solar coronal magnetic field, in view of the base distribution of B_r which varies significantly from the pole to equator. However, a uniform latitudinal distribution of B_r at 1 AU does not necessarily invalidate a scenario where open magnetic fluxes originate from

throughout the Sun. In this regard, we agree with Smith et al. (2001) who concluded that the coronal magnetic field cannot be exactly radial.

4 CONCLUDING REMARKS

Identifying the origin of the Sun's open magnetic flux is of crucial importance in establishing the connection between the in situ solar winds and their sources. In the absence of a definitive measurement of the solar coronal magnetic field, this identification problem is subject to considerable debate (e.g., Schwenn 2006; Wang 2009). This is true even at solar minima when the configuration of the solar corona is relatively simple, with the most prominent feature being the bright streamer helmets in white light images. Although the prevailing view is that the majority of the solar wind originates from outside streamer helmets (Pneuman & Kopp 1971), there also exists the suggestion that the open magnetic field is ubiquitous on the Sun and not confined to coronal holes or the quiet Sun (Woo & Habbal 1999, 2003). Implementing the former scenario in a numerical model has been a common practice (e.g. Lionello et al. 2009), however, so far the latter has not been modeled quantitatively and hence tested quantitatively. Here we offer such an implementation.

We have constructed two 2-dimensional, Alfvénic-turbulence-based models of the solar corona and solar wind, one with and the other without a closed magnetic field region in the inner corona. The purpose of the latter model is to minimize the contribution of the closed magnetic field, trying to mimic a corona permeated with open magnetic fields which may infiltrate the dome-shaped streamer base. In specifying the boundary conditions at the coronal base, we have taken into account some important observational constraints, especially those on the magnetic flux distributions. Interestingly, the two models provide similar pB maps in the FOV of the SOHO/LASCO C2 and C3 coronagraphs. In particular, a dome-shaped feature is present in the C2 FOV even for the model without a closed magnetic field. Moreover, both models fit the Ulysses data scaled to 1 AU equally well. Hence we suggest that: 1) The pB observations cannot be safely taken as a proxy for the magnetic field topology, as is often implicitly assumed. 2) The Ulysses measurements, especially the one indicating that the radial magnetic field strength is nearly uniformly distributed with heliocentric latitude, do not rule out the ubiquity of open magnetic fields on the Sun.

We do not intend to resolve the conflict of the two distinct scenarios currently available for the origin of the heliospheric magnetic flux. Rather, the presented numerical results suggest the likelihood that the magnetic field structure of bright features (e.g., helmet streamers) in the corona may be more diverse than traditionally viewed: the magnetic flux therein can be either closed or open. To differentiate the scenarios, it is likely that more stringent constraints come from the SOHO/UVCS measurements. For instance, measurements based on the Doppler dimming technique have yielded that along the direction transverse to the streamer helmet, there exists a transition in the inferred plasma speed from unmeasurable to significant values, and this transition seems to trace the streamer legs (Strachan et al. 2002; Frazin et al. 2003), identified by the enhancement of the intensity ratio of O VI $\lambda 1032 \text{ \AA}$ to H I Ly α (Kohl et al. 1997). Therefore, it remains to be seen whether a model permeated with open magnetic fluxes can account for this feature. To do this, an obvious need is to incorporate O⁵⁺ ions in a three-fluid model and test both scenarios. At the moment, in such models only the traditional partially open scenario has been adopted (e.g., Li et al. 2006; Ofman et al. 2011). Instead of implementing a further construction, let us end here by noting that one may also ask whether these observational features (Kohl et al. 1997; Strachan et al. 2002; Frazin et al. 2003) are universal for all streamers.

Acknowledgements The Ulysses data were obtained from the CDAWeb database. The two Ulysses teams, SWOOPS (PI: D.J. McComas) and VHM (PI: A. Balogh) are gratefully acknowledged. This research is supported by the National Natural Science Foundation of China (Grant Nos. 40904047 and 41174154), the Ministry of Education of China (20110131110058 and NCET-11-0305), and also by the Specialized Research Fund for State Key Laboratories.

References

- Abbo, L., Antonucci, E., Mikić, Z., et al. 2010, *Advances in Space Research*, 46, 1400
- Altschuler, M. D., & Newkirk, G. 1969, *Sol. Phys.*, 9, 131
- Cargill, P. J. 2009, *Space Sci. Rev.*, 144, 413
- Esser, R., Fineschi, S., Dobrzycka, D., et al. 1999, *ApJ*, 510, L63
- Frazin, R. A., Cranmer, S. R., & Kohl, J. L. 2003, *ApJ*, 597, 1145
- Habbal, S. R., Esser, R., & Arndt, M. B. 1993, *ApJ*, 413, 435
- Habbal, S. R., Woo, R., & Arnaud, J. 2001, *ApJ*, 558, 852
- Habbal, S. R., Arndt, M. B., Nayfeh, M. H., et al. 2003, *ApJ*, 592, L87
- Hu, Y. Q., Habbal, S. R., Chen, Y., & Li, X. 2003, *Journal of Geophysical Research (Space Physics)*, 108, 1377
- Kohl, J. L., Noci, G., Antonucci, E., et al. 1997, *Sol. Phys.*, 175, 613
- Kopp, R. A. 1994, *Space Sci. Rev.*, 70, 309
- Levine, R. H., Altschuler, M. D., & Harvey, J. W. 1977, *J. Geophys. Res.*, 82, 1061
- Li, B., Li, X., & Labrosse, N. 2006, *Journal of Geophysical Research (Space Physics)*, 111, A08106
- Li, J., Raymond, J. C., Acton, L. W., et al. 1998, *ApJ*, 506, 431
- Lin, H., Kuhn, J. R., & Coulter, R. 2004, *ApJ*, 613, L177
- Lionello, R., Linker, J. A., & Mikić, Z. 2009, *ApJ*, 690, 902
- Liu, Y. 2009, *Annales Geophysicae*, 27, 2771
- McComas, D. J., Barraclough, B. L., Funsten, H. O., et al. 2000, *J. Geophys. Res.*, 105, 10419
- Neugebauer, M., Forsyth, R. J., Galvin, A. B., et al. 1998, *J. Geophys. Res.*, 103, 14587
- Neugebauer, M., Liewer, P. C., Smith, E. J., Skoug, R. M., & Zurbuchen, T. H. 2002, *Journal of Geophysical Research (Space Physics)*, 107, 1488
- Ofman, L., Abbo, L., & Giordano, S. 2011, *ApJ*, 734, 30
- Pneuman, G. W., & Kopp, R. A. 1971, *Sol. Phys.*, 18, 258
- Schatten, K. H., Wilcox, J. M., & Ness, N. F. 1969, *Sol. Phys.*, 6, 442
- Schwenn, R. 2006, *Space Sci. Rev.*, 124, 51
- Smith, E. J., & Balogh, A. 1995, *Geophys. Res. Lett.*, 22, 3317
- Smith, E. J., Balogh, A., Forsyth, R. J., & McComas, D. J. 2001, *Geophys. Res. Lett.*, 28, 4159
- Strachan, L., Suleiman, R., Panasyuk, A. V., Biesecker, D. A., & Kohl, J. L. 2002, *ApJ*, 571, 1008
- Svalgaard, L., Duvall, T. L., Jr., & Scherrer, P. H. 1978, *Sol. Phys.*, 58, 225
- Tadesse, T., Wiegmann, T., & Inhester, B. 2009, *A&A*, 508, 421
- van de Hulst, H. C. 1950, *Bull. Astron. Inst. Netherlands*, 11, 135
- Vásquez, A. M., van Ballegoijen, A. A., & Raymond, J. C. 2003, *ApJ*, 598, 1361
- Wang, Y.-M. 2009, *Space Sci. Rev.*, 144, 383
- Wang, Y.-M., & Sheeley, N. R., Jr. 1990, *ApJ*, 355, 726
- Wang, Y.-M., & Sheeley, N. R., Jr. 2006, *ApJ*, 653, 708
- Woo, R., & Druckmüllerová, H. 2008, *ApJ*, 678, L149
- Woo, R., & Habbal, S. R. 1999, *ApJ*, 510, L69
- Woo, R., & Habbal, S. R. 2003, in *Solar Wind Ten*, American Institute of Physics Conference Series, 679, eds. M. Velli, R. Bruno, F. Malara, & B. Bucci (New York: AIP), 55
- Woo, R., Habbal, S. R., & Feldman, U. 2004, *ApJ*, 612, 1171
- Zhao, X., & Hoeksema, J. T. 1995, *J. Geophys. Res.*, 100, 19